Dalton Transactions

PAPER

View Article Online
View Journal | View Issue

Cite this: *Dalton Trans.*, 2014, **43**, 698

Ligand spheres in asymmetric hetero Diels–Alder reactions catalyzed by Cu(II) box complexes: experiment and modeling†

V. Umamaheswari,[a] Pawel Cias,[a] Andreas Pöppl,[b] Martin Kaupp[c] and Georg Gescheidt*[a]

Received 17th June 2013,
Accepted 13th September 2013

DOI: 10.1039/c3dt51602d

www.rsc.org/dalton

The stereoselective hetero Diels–Alder reaction between ethyl glyoxylate and cyclohexadiene catalyzed by [Cu(II)*t*-Bu-(box)](OTf)$_2$ was investigated. The reaction was performed step-by-step and the geometry of the Cu(II) complexes formed in the course of the catalysis was analysed by EPR spectroscopy, advanced pulsed EPR methods (ENDOR, and HYSCORE) and DFT calculations. Our results show that one triflate counterion is directly coordinated to Cu(II) during the catalytic process (axial position). This leads to penta-coordinated Cu(II) complexes. Solvent molecules are able to alter the geometry of the Cu(II) complexes although their coordination is weak. These findings provide an explanation for the solvent and counterion effects observed in many catalytic reactions.

1. Introduction

Stereoselective catalysis provides an efficient access for the construction of complex molecules containing chiral centers.[1–4] A prominent strategy to introduce C–C bonds into even complex molecular skeletons is the Diels–Alder reaction. It is well known that the presence of Lewis acids activates dienophiles and leads to a substantial enhancement of the conversion.[5,6] In particular, Cu(II) complexes carrying chiral ligands have been shown to be very efficient catalysts.[1,7,8] Here, C_2-symmetric bis(oxazoline) (box) derivatives have been particularly successful.[2,9–18] and a number of related molecules binding to Cu(II) *via* two nitrogen atoms have been developed.[19–24] However, not only the nature of the ligand but also the solvent and counterions play a decisive role in the efficiency and stereoselectivity of the catalytic reactions.[25–30] This is particularly reflected in the recent developments of ligand design and the involvement of alternative counterions.[31,32]

Nevertheless, mechanistic details in terms of the arrangement of ligands are scarce. In the models utilized for theoretical investigations,[30,33–40] stereoselectivity is particularly ascribed to steric effects in tetracoordinated Cu(II) environments; counterion and solvent effects are mostly neglected. A recent study of Cu(II)box complexes shows that environmental effects are crucial.[41]

EPR studies provide rather precise insights into the geometry of transition-metal complexes.[42,43] For Cu(II) bis(sulfoximine) complexes, we have shown that penta coordination occurs in the course of (hetero) Diels–Alder reactions, with counterions and solvent molecules participating in the first coordination sphere.[44,45] A compatible geometry was found by X-ray analysis in the complex [Cu(II)*t*-Bu(box)(OH$_2$)$_2$](OTf)$_2$.[10] The question is whether such an arrangement of ligands (penta-coordination) represents a general concept within the course of Cu(II) catalyzed Diels–Alder reactions. We therefore investigated a hetero Diels–Alder reaction under "real conditions". This means that we utilised frequently used substrates and performed the reactions under synthetic conditions. Ethyl glyoxylate (**1**) serves as the dienophile which adds to cyclohexadiene (**2**) with [Cu(II)*t*-Bu(box)](OTf)$_2$ as the catalyst in CH_2Cl_2 (the most commonly used solvent, Scheme 1). The reaction is followed stepwise by EPR spectroscopy. The shape of the solid-state continuous-wave EPR spectra indicates whether a paramagnetic system has a high or low symmetry (*e.g.* axial symmetry). Interactions between the Cu(II) and its nearest neighbors can be derived from anisotropic hyperfine coupling constants (HFCs). In experimental EPR spectra the corresponding splittings are often not resolved. To obtain precise, orientation-dependent HFC values, we utilized pulsed ENDOR (electron nuclear double resonance)[46] and

[a]*Institute of Physical and Theoretical Chemistry, Graz University of Technology, Stremayrgasse 9, 8010 Graz, Austria. E-mail: g.gescheidt-demner@tugraz.at; Fax: (+43)316 873 32202*
[b]*Faculty of Physics and Earthscience, University of Leipzig, Linnéstr. 5, D-04103, Leipzig, Germany*
[c]*Technische Universität Berlin, Fakultät II, Institut für Chemie, Strasse des 17, Juni 135, 10623 Berlin, Germany*
†Electronic supplementary information (ESI) available. See DOI: 10.1039/c3dt51602d

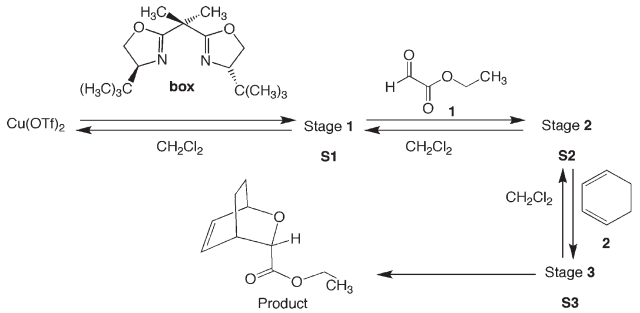

Scheme 1 A model hetero Diels–Alder reaction.

HYSCORE (hyperfine sub-level correlation).[47] With the help of theoretical DFT calculations, which also provide EPR parameters, these experimental parameters can be translated into the geometry of the chemical environment around the paramagnetic Cu(II) center.[48–52]

2. Experimental

Sample preparation: the $Cu(OTf)_2$ and (*S*)-(−)-2,2′-isopropylidenebis(4-*tert*-butyl-2-oxazoline) ligand were dissolved in dry CH_2Cl_2 in a molar ratio of 1 : 1.2 and stirred for 3 hours under argon to form the catalyst, [Cu(II)*t*-Bu(box)]$(OTf)_2$ in solution. Part of this solution was transferred to the quartz X-band EPR sample tube, degassed by three freeze–pump–thaw cycles and sealed. This forms the catalyst sample (sample **S1**). Then ethyl glyoxylate in seven fold molar excess was added to the catalyst solution and part of this solution was transferred to another EPR sample tube under argon, degassed and sealed. This forms the sample **S2**. To the solution forming sample **S2**, 1,3-cyclohexadiene was added in a four fold molar excess to that of ethyl glyoxylate, and this solution was transferred into the EPR sample tube under argon, degassed and sealed. This forms the sample **S3**. EPR measurements: the CW and pulsed EPR measurements were performed using X-band (ν_{mv} = 9.7 GHz) BRUKER ELEXYS E580 and ESP 380 spectrometers. The CW EPR spectra were recorded at 7 K using an Oxford He flow cryostat. The B_0 modulation amplitude used was 0.4 mT, and the modulation frequency was adjusted to ν_{mod} = 100 kHz. The microwave power used was low enough to prevent the saturation of spin systems. The simulations of the CW EPR spectra were done using the Easyspin simulation package.[53] Two pulse field-swept electron spin echo (FS ESE) experiments were carried out at 4 K using microwave pulses with pulse lengths of 16 ns for π/2 and 32 ns for π pulses and a pulse delay of τ = 160 ns. Orientation-selective two dimensional ESEEM experiments were performed at 4 K using the HYSCORE[54] sequence (π/2-τ-π/2-t_1-π-t_2-π/2-τ-echo). Pulse lengths of 16 ns for π/2 and 32 ns for π pulses were employed and three different pulse delays of τ = 32, 104 and 160 ns were chosen in the 2D experiments to minimize blind spots in the HYSCORE powder patterns. Since the dead time of the spectrometer exceeds 32 ns in our experimental setup, in the case of τ = 32 ns the HYSCORE echo was detected *via* a remote echo sequence (π/2-τ_R-π/2-τ_R-π-τ_R-echo).[55] The pulse delays of remote echo sequence were t_R = 4 μs and τ_R = 140 ns. A four-step phase cycle suggested by Gemperle *et al.*[56] was used to avoid interference with the unwanted two- and three-pulse echoes. A 170 × 170 2D data matrix was sampled with a dwell time of 16 ns. Baseline correction was done by subtracting a third-order polynomial of the experimental data set in both time domains. Finally, the HYSCORE spectra recorded with different τ values were added and the 2D FT magnitude spectra were calculated and presented as contour plots. The simulations of the HYSCORE spectra were calculated in the time domain by exact diagonalization of the spin Hamiltonian. Subsequently, the computed time domain spectra were likewise zero filled and transformed into the frequency domain by Fast Fourier Transformation. For further information concerning the procedure for the calculation of orientation selective HYSCORE spectra, we refer to the paper by Pöppl *et al.*[57] Selective microwave pulses of $t_{\pi/2}$ = 96 and t_π = 192 ns, and a radiofrequency pulse length of t_{rf} = 8 μs were used in orientation selective Davies pulsed ENDOR experiments.[46] In an effort to suppress both the proton and the fluorine signals and enhance those from the two imine nitrogen atoms (from the *t*-Bu-box ligand) with substantially larger hyperfine couplings (HFC) involved in the coordination with the Cu(II), additional hyperfine contrast selective ENDOR experiments were done with $t_{\pi/2}$ = 16 and t_π = 32 ns.

The geometries of [Cu(II)*t*-Bu(box)]$(OTf)_2$ and [Cu(II)*t*-Bu(box)(ethyl glyoxylate)](OTf) complexes used for the hyperfine structure and g-tensor computations were optimized in unrestricted Kohn–Sham calculations at the B3LYP[58–60] level using the Turbomole package.[61] The basis sets were of polarized triple-ζ quality for all atoms (TZVP).[62] The same holds for the calculations of the energetic effects of **S3** formation. All hyperfine calculations were carried out with the ORCA[63] program package at the optimized geometries and using hybrid B3LYP functional. The choice of this functional was based on previous computations which show that it is very successful in the prediction of hyperfine coupling (HFC) and g-tensor in nitrogen and Cu(II) complexes.[48,64–66] Ligand atoms were treated by Huzinaga–Kutzelnigg type basis sets BII (denoted also as IGLO-II).[67,68] For the Cu center an accurate triply polarized basis set CP(PPP) was employed.[69] This basis set is especially flexible in the core region and is believed to provide results close to the basis set limit for the Fermi contact interaction. Because the spin–orbit effects are known to influence the HFC results for 3d transition metal complexes, in the case of the copper atom the contributions of spin–orbit coupling (SOC) to the HFC were taken into account. It was proven that the implementation of SOC contributions into the HFC computations results in a significant improvement of calculated parameters when compared to experiment.[48,66] The calculation of g-tensor values was carried out with the same geometry and basis sets. A common gauge at the copper atom was employed.

3. Results and discussion

EPR ENDOR/HYSCORE and calculations

General – cw EPR Spectra: Frozen-solution EPR spectra obtained at each single reaction stage (**S1**, **S2**, and **S3**, Scheme 1) exhibit differences (Fig. 1). Whereas for stage **S1** one EPR signal is recorded, the spectra taken after addition of **1** (**S2**) and subsequently **2** (**S3**) indicate an overlay of two components (one resembling the preceding stage). The shapes of these spectra were reproducible in several runs and are very likely based on equilibria connecting the different stages of the reaction (for simulations and *g*-factors, see ESI†). In the following sections we will describe and discuss the experimental and calculated EPR parameters of **S1**–**S3**.

Reaction stage **S1**: the complex of *t*-Bu-box with Cu(II) triflate has been described frequently since it is the basis of several catalyses. Based on the shape of the EPR signal (Fig. 1), the complex between $Cu(OTf)_2$ and the *t*-Bu-box (box) ligand **S1** reveals a pseudo axial symmetry. Corresponding HYSCORE spectra taken at the perpendicular and the parallel region (Fig. 2a and b, respectively) reveal the hyperfine coupling constants shown in Table 1. From the above obtained constants, substantial distances between the Cu center and some of the Fand H nuclei (indicated in Fig. 3) could be inferred (Table 2).

To do so, a clear-cut assignment of EPR coupling constants was accomplished. In this context it was of benefit, that, according to the calculations, only few distinct atoms revealed characteristic coupling constants. This was particularly the case for protons at the 4-positions of the box ligand (H^1 in Fig. 3) and the F atoms in the triflate counterions. This finding essentially holds for all ligand spheres we have taken

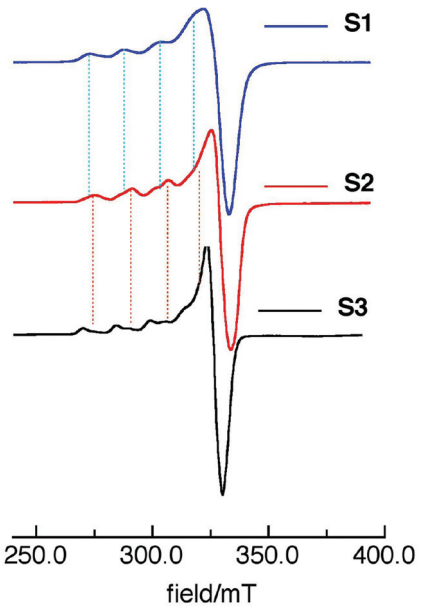

Fig. 1 X-band CW EPR spectra obtained in the course of the reaction sequence displayed in Scheme 1 corresponding to **S1**, **S2**, and **S3**. The dotted lines point to the presence of lines stemming from the preceding EPR spectrum in **S2** and **S3**.

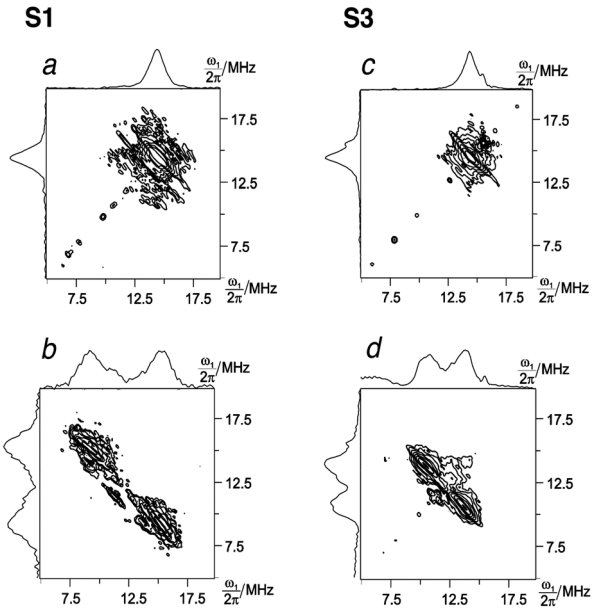

Fig. 2 Comparison of HYSCORE spectra of stage **S1** and **S3** at selected orientations in the EPR spectra (a, perpendicular region of **S1**; b, parallel region of **S1**; c, perpendicular region of **S3**; d, parallel region of **S3**).

Table 1 Experimental and calculated EPR parameters used for the determination of the geometry of **S1** (Scheme 1)

	$A_\perp$/MHz		$A_\parallel$/MHz		A_{iso}/MHz	
	Exp.	Calc.	Exp.	Calc.	Exp.	Calc.
^{63}Cu	37	66	464	−487		
$^{14}N^a$	34	29	40	39	36	32
$^{1}H^1$	−1.18	1.19	8.75	7.17	2.13	2.75
$^{1}H^2$	−2.28	−1.85	5.31	5.77	0.25	0.75
$^{19}F^1$	−2.23	−1.04	7.16	5.63	0.9	1.42
$^{19}F^2$	−2.30	−1.14	2.80	1.28	−0.6	−0.12

[a] The values for the ^{14}N hfc have an error of ±4 MHz based on contrast-selective ENDOR, *cf.* ESI.

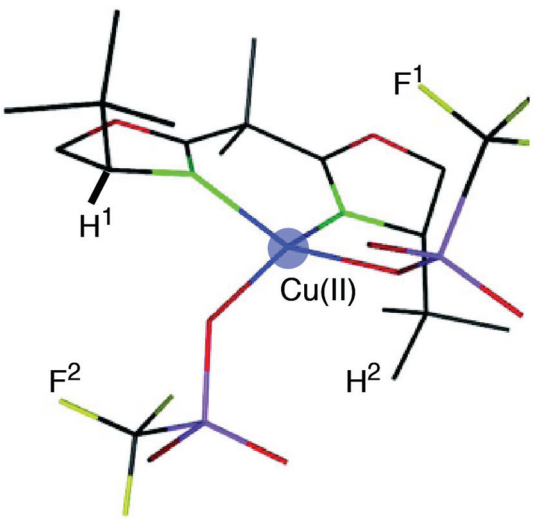

Fig. 3 Calculated geometry of [Cu(II)*t*-Bu(box)](OTf)$_2$.

Table 2 Comparison of selected experimental and calculated Cu(II)···H and Cu(II)···F distances (*r*) in **S1**. (For numbering, see Fig. 3)

Atoms	*r* (EPRDipolexp)/pm	*r* (calc.)/pm
Cu···H[1]	316	311
Cu···H[2]	280	291
Cu···F[1]	294	352
Cu···F[2]	360	353

into account here, and substantially simplified the analysis of the experimental data. Thus, distances could be determined *via* a point-dipole approximation from the dipolar hyperfine coupling constants (HFC) obtained from HYSCORE spectroscopy (see ESI†). These results, in principle, confirm the formerly established structure of the *t*-Bu-box ligand. In order to support these spectroscopic data, however, we have computed the geometry of **S1** using the B3LYP/TZVP protocol. In line with the X-ray structure determinations and the EPR data, Cu(II) is surrounded by the two imino nitrogen atoms of the box ligand and two oxygens of the OTf^- counterions at (quasi) equatorial positions. The geometry is displayed in Fig. 3 and selected distances are summarized in Table 2.

To investigate whether the calculated geometries correspond to those from the X-ray analysis we calculated the well-described complex $[Cubox]Cl_2$ as a reference. As shown in the ESI,† the calculated and the experimental geometry are virtually matching. Accordingly, the computed geometries can be regarded as very suitable predictions for the experimental data. Moreover, in Table 3, the calculated values are compared with experimentally determined data of related Cu(II)-box derivatives.[10,37]

The experimental and the DFT-calculated distances and angles for this reference agree rather well (Table 3) and are in line with X-ray structure data of related complexes.[37,70]

Reaction stages **S2** and **S3**: the EPR spectra taken for these two stages reveal almost matching ^{63,65}Cu coupling constants (**S2**: $A_{\|}$ = 424, $A_{\perp}$ = 38 MHz: **S3**: $A_{\|}$ = 460, $A_{\perp}$ = 38 MHz) indicating pseudo-axial symmetry. Moreover, the HYSCORE resonances obtained from **S2** and **S3** are basically identical. It can, therefore, be assumed that the first ligand sphere around Cu(II) cation remains essentially unchanged when the diene is added to **S2**, *i.e.* only the (activated) dienophile reveals direct bonding with Cu(II) center. Therefore, we discuss the structure of **S2** and **S3** jointly. For computational reasons it is more straightforward to develop **S2** first and then to add the diene,

Table 3 Comparison of relevant interatomic distances of calculated [Cu(II)*t*-Bu-(box)](OTf)$_2$ and [Cu(II)*t*-Bu(box)]Cl$_2$ complexes with reported X-ray data[a]

	Cl	Cl[a]	OTf	OTf[a]
Cu–N (pm)	200.6	198.3	202.4	196.1
N–Cu–N (°)	90.9	90.5	90.1	93.6
Cu-ligand (pm)	224.7	223.2	195.4	195.9

[a] Ref. 35.

Table 4 Experimental EPR parameters used for the simulation of the EPR and the HYSCORE spectra attributed to **S2** (Scheme 1) and calculated data[a]

	$A_{\perp}$/MHz		$A_{\|}$/MHz		A_{iso}/MHz	
	Exp.	Calc.	Exp.	Calc.	Exp.	Calc.
^{63}Cu	38	52	424	−536		
^{14}N[b]	32	36	48	49	37	41
^{1}H	−1.46	−1.4	6.82	4.6	1.3	0.5
^{19}F	−0.73	−0.6	1.46	1.19	0.0	0.0

[a] See text for the explanation of the ligand spheres. [b] The values for the ^{14}N hfc have an error of ±4 MHz based on contrast-selective ENDOR, *cf.* ESI.

to obtain **S3**. The HYSCORE spectra particularly reveal two clearly discernible interactions: one set of ^{1}H coupling constants ($A_{\|}$ = 6.82, $A_{\perp}$ = −1.46 MHz), one of ^{19}F ($A_{\|}$ = 1.46, $A_{\perp}$ = −0.73 MHz), and of ^{14}N ($A_{\|}$ = 48, $A_{\perp}$ = 32 MHz, also corroborated by ENDOR). These experimental data have to be compared to their calculated counterparts to obtain the shapes of the ligand spheres (see Table 4). The ^{14}N hfc of the two bis (oxazoline) nitrogens compares very well with its calculated counterpart (A_{iso} 37 MHz, *vs.* 41 MHz). The hfc values of the ^{63}Cu center also agree closely with the calculated ones ($A_{\perp}$ = 38 MHz, $A_{\|}$ = 424 *vs.* 52 and −536 MHz, respectively). The same holds for the biggest ^{1}H hfc of $A_{\perp}$ = −1.46 $A_{\|}$ 6.82 MHz (calc.: −1.40 and 4.60 MHz, resp.) and the ^{19}F hfc of $A_{\perp}$ = −0.73 $A_{\|}$ = 1.46 MHz (calc.: −0.60 and 1.19 MHz, resp.) which also translates into a Cu···F distance of 477 pm (calc., 483 pm). A comparison with published investigations on the popular Cu(II) bis(oxazoline)-based catalytic systems is in place here. In most cases, the mechanism of Diels–Alder reactions performed in the way shown in Scheme 1 is implied to proceed *via* tetra coordinate 17-electron stages with the box ligand and a substrate molecule (the dienophile) coordinated to Cu(II). This concept was followed in computational approaches.[33,34,37] Rarely were solvent molecules explicitly taken into account.[37] Stereoselectivity has been predominately ascribed to the steric congestion of the substituents at the 4.4′ position in the 1,3-bisoxazoline rings; moreover it has been emphasized that the constitutional flexibility and the dynamics of the ligands play an important role in stereoselectivity.[37] Pentacoordination was reported in the course of catalyses performed in zeolites containing the Cu(II) box complexes[43] and in enantioselective aldol reactions with [(Cu(II)S,S)-pybox](OTf)^2,[71] where the five ligand atoms originate from the three nitrogens of a pyridylbox ligand and the two oxygens of a glyoxylate. Moreover enzymes, *e.g.* galactose oxidase display penta-coordinated Cu(II) centers.[72,73] With this background, we have calculated models for ligand spheres **S2** but unlike for [Cu(II)*t*-Bu(box)](OTf)$_2$, in this case, both the counterion and solvent molecules are taken into account. Three different environments are constructed. They mirror the composition of the reaction mixture and the experimentally established finding that pentacoordination exists around Cu(II)

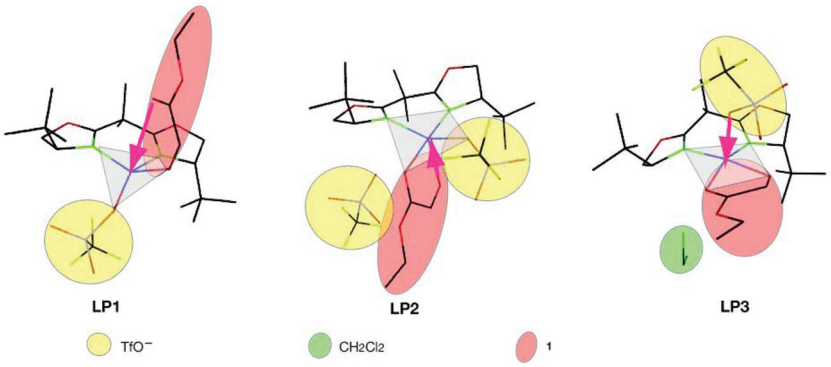

Fig. 4 Calculated geometries for ligand spheres **LP1–LP3**. The grey shades indicate the equatorial, square-type coordination whereas the arrows highlight the axial oxygen atom, which for **LP1** and **LP2** is provided by ethyl glyoxylate **1** and for **LP3** by one of the triflate oxygens.

(Fig. 4). For all calculations, the ligands were placed at clearly non-bonding distances (<500 pm away from Cu(II)) as the starting point and geometry optimizations were performed without any constraints. The first ligand sphere (**LP1**, Fig. 4) comprises the *t*-Bu-box ligand, and ethyl glyoxylate (**1**) and one triflate anion representing an 18-electron complex providing two N, and three oxygen atoms for coordination to Cu(II). However, geometry optimization with this combination leads to a basically tetra-coordinate ligand sphere with an essentially tetrahedral arrangement consisting of the two *t*-Bu-box N atoms (N_I, N_{II}, Fig. 5), and two O atoms provided by the OTf^- and the aldehyde oxygen of ethyl glyoxylate (O_{D2}, O_T, Fig. 5). The second carbonyl oxygen belonging to the dienophile resides at a significantly longer distance from the Cu(II) center (314 pm) and can hardly be regarded as a coordinating ligand (O_{D1}). Moreover, this structure is not consistent with the experimental results, which indicate that ethyl glyoxylate is coordinated equatorially through its carbonyl oxygens in a bidentate fashion while the triflate ligand is attached to the Cu center in the axial position through the sulfonic oxygen atom (revealed by the experimentally established Cu(II)···F distance). In **LP2** (Fig. 4) one additional OTf^- anion is added to the components of **LP1**, to test the influence of charge compensation by two counterions. This indeed leads to pentacoordination of Cu(II) with *t*-Bu-box N atoms (N_I, N_{II}), both glyoxylate carbonyl oxygen atoms (O_{D1}, O_{D2}) and one triflate oxygen (O_T). The second OTf^- resides at a distant position without directly interacting with Cu(II). Again, there is a significant mismatch between this calculated structure and the experimental data. Only one carbonyl oxygen lies in the equatorial plane (O_{D2}), while the other (O_{D1}) acts as the axial ligand. In contrast to the findings by HYSCORE the triflate is coordinated at an equatorial position. Finally, since it has been observed that CH_2Cl_2 is a particularly good solvent for these catalyses and an additional triflate does not coordinate directly but leads to a geometry change of the complex,[1] **LP3** was constructed the following way: it includes one *t*-Bu-box ligand, ethyl glyoxylate, one triflate anion and, explicitly, one solvent molecule (CH_2Cl_2, Fig. 4). The optimized environment of **LP3**, shows an equatorial (distorted) square formed by the two *t*-Bu-box N atoms (N_I, N_{II}), the two carbonyl O atoms of ethyl glyoxylate (O_{D1}, O_{D2}). Importantly, one oxygen atom of the triflate anion (O_T) serves as an axial ligand at a distance of 226/223 pm (**S2**/**S3**). This arrangement is, in fact, consistent with the experimental data. Table 5 presents a comparison between the experimental and the calculated interatomic distances Cu···F, Cu···H[2] (for numbering of the H-atom, see Fig. 3), for **LP1**, **LP2**, and **LP3**) together with the ϑ angles with respect to g_{zz} axis. Essential computed geometrical parameters of the complexes **LP1**, **LP2**, and **LP3** in Cu(II) center proximity are listed in Table 6.

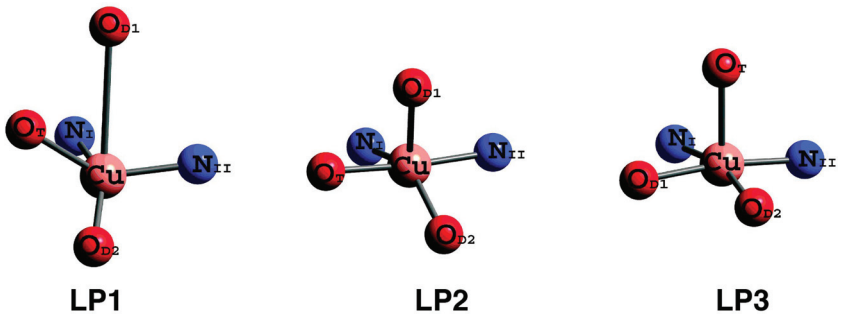

Fig. 5 Detailed view of the first coordination sphere around Cu(II) calculated for **LP1–LP3**. Calculated by DFT at B3LYP/TZVP level. N_I and N_{II} illustrate two nitrogen atoms of box, O_T – oxygen atom coming from the triflate anion. O_{D1}, O_{D2} depict two oxygen atoms of ethyl glyoxylate. The most relevant bond lengths and dihedrals on which the comparison with the experiment is based are listed in Table 6.

Table 5 Calculated and experimental interatomic distances Cu···H^2 and Cu···F distances for **LP1**, **LP2** and **LP3**. Also given: θ angles of F and H nuclei with respect to g_{zz} axis

	LP1	LP2	LP3 (S2/S3)	Exp.
H^2 θ (°)	40	60	52/52	51
Cu···H^2 (pm)	351	320	317/316	307
F θ (°)	25	36	26/28	32
Cu···F (pm)	486	471	483/480	477

Table 6 Essential bond lengths and dihedrals in Cu proximity for **LP1**, **LP2** and **LP3** (Fig. 5) calculated by DFT

	LP1	LP2	LP3 (S2/S3)
Dihedral (°)			
N_I–Cu–N_{II}–O_{D2}	139	175	174/174
N_{II}–Cu–N_I–O_{D1}	76	102	166/167
N_I–Cu–N_{II}–O_T	155	144	99/99
Distance (pm)			
Cu···O_{D1}	314	233	206/205
Cu···O_{D2}	223	202	208/210
Cu···O_{DT}	190	202	226/223

Energetic effects found with the final stage **S3** of the reaction was also calculated for all three structures. The calculations confirm a high feasibility of the **LP3** geometry (ΔE = −12.4 kcal mol^{-1})) and render **LP2** very unfavorable (ΔE = 0.9 kcal mol^{-1}). The structure **LP1** is favorable from the energetic point of view (ΔE = −9.3 kcal mol^{-1}), however, as shown above, the calculated EPR parameters are not in such a good agreement with the experiments like **LP3**. Deeper insight into the structures and coordination spheres could be provided by the calculations of full reaction pathways including the computations of the transition states. In the case of calculations of transition state structures containing counterions and solvent molecules, however, it was not possible to eliminate imaginary frequencies corresponding to their relative motions. These modes obviously caused the deviation in the TS energy of the complexes. Due to this inaccuracy this part of the study is still in progress and will be published in the next paper. Luckily the calculations of the EPR parameters were free of such incorrectness.

4. Conclusions

In several investigations based on product analysis, a distorted square-type ligand sphere formed by the two N atoms of a box-type ligand and two O atoms of the substrate (**1**) has generally been suggested.[1] Our results, however, show that penta-coordination at Cu(II) is potentially decisive in the course of stereoselective (hetero) Diels–Alder reactions. One triflate counterion acts as an additional axially oriented ligand providing an 18-electron complex. Our calculations show that even (weakly coordinating) solvent molecules have a subtle impact on the geometry of the catalytically-active complex. Numerous

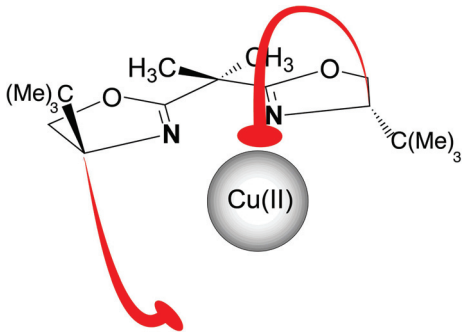

Fig. 6 Suggested ligand modifications on a box ligand leading to higher catalytic efficiency.

publications on stereoselective catalyses reveal that the efficiency of these reactions substantially depends on the parent Cu(II) salt and the solvent used. Our results lead to the following suggestions: (i) an efficient ligand providing an additional site for axial coordination should diminish the counterion dependence. (ii) One additional weakly binding group should decrease the influence of the solvent. These structural features are displayed in Fig. 6. These results could serve as a basis for the development of efficient catalytic systems and may open an additional starting point for the modeling of enzymatic activity.[36]

Our results elucidate the observations from the synthesis: it was shown that box ligands with (4,4′-sulfonamidomethyl) substituents allowing additional coordination sites (*i.e.* penta-coordination)[7] show higher conversion and stereoselectivity even in the strongly coordinating solvent $MeNO_2$.[74] Efficient penta-coordinate arrangements were shown for Cu(II)-containing tripodal bis(oxazoline) ("trisox") derivatives[75] and enzymes,[51,72,73] and recent NMR investigations show that solvents and counterions substantially influence the geometry of the transition-metal complexes in solution.[76]

Establishing the transition state responsible for the formation of the Diels–Alder adduct in the presence of solvent and counterion molecules will be the next step of our investigations. The most likely starting point will be the geometry found for state **S3**, however, the complexity of such an environment around the Cu center makes these calculations highly challenging and demanding. We are now further elaborating this concept by experiment and, particularly, by theory.

Acknowledgements

Financial support for this work by the Austrian Science Fund (FWF), Project no. P19711 is gratefully acknowledged.

References

1 S. Reymond and J. Cossy, *Chem. Rev.*, 2008, **108**, 5359–5406.
2 G. Desimoni, G. Faita and K. A. Jorgensen, *Chem. Rev.*, 2006, **106**, 3561–3651.

3 R. Rasappan, D. Laventine and O. Reiser, *Coord. Chem. Rev.*, 2008, **252**, 702–714.
4 D. A. Evans, J. S. Johnson and E. J. Olhava, *J. Am. Chem. Soc.*, 2000, **122**, 1635–1649.
5 S. Yao, M. Roberson, F. Reichel, R. G. Hazell and K. A. Jørgensen, *J. Org. Chem.*, 1999, **64**, 6677–6687.
6 M. Johannsen, K. A. Jørgensen, X.-F. Zheng, Q.-S. Hu and L. Pu, *J. Org. Chem.*, 1999, **64**, 299–301.
7 A. Sakakura, R. Kondo, Y. Matsumura, M. Akakura and K. Ishihara, *J. Am. Chem. Soc.*, 2009, **131**, 17762–17764.
8 M. Yu and S. J. Danishefsky, *J. Am. Chem. Soc.*, 2008, **130**, 2783–2785.
9 A. Landa, B. Richter, R. L. Johansen, A. Minkkilae and K. A. Jorgensen, *J. Org. Chem.*, 2007, **72**, 240–245.
10 D. A. Evans, C. S. Burgey, N. A. Paras, T. Vojkovsky and S. W. Tregay, *J. Am. Chem. Soc.*, 1998, **120**, 5824–5825.
11 D. A. Evans, M. C. Kozlowski and J. S. Tedrow, *Tetrahedron Lett.*, 1996, **37**, 7481–7484.
12 D. H. Ryu, G. Zhou and E. J. Corey, *J. Am. Chem. Soc.*, 2004, **126**, 4800–4802.
13 A. S. Gokhale, A. B. E. Minidis and A. Pfaltz, *Tetrahedron Lett.*, 1995, **36**, 1831–1834.
14 A. K. Ghosh, P. Mathivanan, J. Cappiello and K. Krishnan, *Tetrahedron: Asymmetry*, 1996, **7**, 2165–2168.
15 A. Pfaltz, *Acta Chem. Scand.*, 1996, **50**, 189–194.
16 J. M. Takacs, D. A. Quincy, W. Shay, B. E. Jones and C. R. Ross II, *Tetrahedron: Asymmetry*, 1997, **8**, 3079–3087.
17 M. Johannsen, S. Yao, A. Graven and K. A. Jorgensen, *Pure Appl. Chem.*, 1998, **70**, 1117–1122.
18 H. Pellissier, *Tetrahedron*, 2009, **65**, 2839–2877.
19 I. Atodiresei, I. Schiffers and C. Bolm, *Tetrahedron: Asymmetry*, 2006, **17**, 620–633.
20 C. Bolm, M. Verrucci, O. Simic, P. G. Cozzi, G. Raabe and H. Okamura, *Chem. Commun.*, 2003, 2826–2827.
21 C. Bolm and O. Simic, *J. Am. Chem. Soc.*, 2001, **123**, 3830–3831.
22 K. A. Jorgensen, M. Johannsen, S. L. Yao, H. Audrain and J. Thorhauge, *Acc. Chem. Res.*, 1999, **32**, 605–613.
23 M. Gomez, G. Muller and M. Rocamora, *Coord. Chem. Rev.*, 1999, **193–195**, 769–835.
24 N. Hutabarat, C. Seki, T. Shimizu, M. Hirama, Y. Kohari, H. Nakano, K. Uwai, N. Takano, E. Kwon and H. Matsuyama, *Heterocycles*, 2012, **86**, 203–217.
25 O. Acevedo and W. L. Jorgensen, *J. Chem. Theory Comput.*, 2007, **3**, 1412–1419.
26 M. Johannsen and K. A. Jorgensen, *J. Chem. Soc., Perkin Trans. 2*, 1997, 1183–1185.
27 M. Johannsen and K. A. Joergensen, *Tetrahedron*, 1996, **52**, 7321–7328.
28 A. Schaetz, R. Rasappan, M. Hager, A. Gissibl and O. Reiser, *Chem.–Eur. J.*, 2008, **14**, 7259–7265.
29 A. Macchioni, *Chem. Rev.*, 2005, **105**, 2039–2073.
30 J. M. Fraile, J. I. Garcia, M. J. Gil, V. Martinez-Merino, J. A. Mayoral and L. Salvatella, *Chem.–Eur. J.*, 2004, **10**, 758–765.
31 A. Sakakura and K. Ishihara, *Chem. Soc. Rev.*, 2011, **40**, 163–172.
32 S. Antoniotti, V. Dalla and E. Dunach, *Angew. Chem., Int. Ed.*, 2010, **49**, 7860–7888.
33 A. E. Hayden, J. DeChancie, A. H. George, M. Dai, M. Yu, S. J. Danishefsky and K. N. Houk, *J. Org. Chem.*, 2009, **74**, 6770–6776.
34 J. DeChancie, O. Acevedo and J. D. Evanseck, *J. Am. Chem. Soc.*, 2004, **126**, 6043–6047.
35 R. K. Jangid, N. Gupta, R. K. Bansal, M. von Hopffgarten and G. Frenking, *Tetrahedron Lett.*, 2011, **52**, 1721–1724.
36 J. B. Siegel, A. Zanghellini, H. M. Lovick, G. Kiss, A. R. Lambert, J. L. S. Clair, J. L. Gallaher, D. Hilvert, M. H. Gelb, B. L. Stoddard, K. N. Houk, F. E. Michael and D. Baker, *Science*, 2010, **329**, 309–313.
37 J. Thorhauge, M. Roberson, R. G. Hazell and K. A. Joergensen, *Chem.–Eur. J.*, 2002, **8**, 1888.
38 P. Moerschel, J. Janikowski, G. Hilt and G. Frenking, *J. Am. Chem. Soc.*, 2008, **130**, 8952–8966.
39 *Theoretical calculations of metal-catalyzed cycloaddition reactions*, ed. K. A. Jorgensen, Wiley, New York, 2002.
40 Y.-h. Lam, P. H.-Y. Cheong, J. M. Blasco Mata, S. J. Stanway, V. Gouverneur and K. N. Houk, *J. Am. Chem. Soc.*, 2009, **131**, 1947–1957.
41 M. E. Owen, E. Carter, G. J. Hutchings, B. D. Ward and D. M. Murphy, *Dalton Trans.*, 2012, **41**, 11085–11092.
42 S. Van Doorslaer, I. Caretti, I. A. Fallis and D. M. Murphy, *Coord. Chem. Rev.*, 2009, **253**, 2116–2130.
43 Y. Traa, D. M. Murphy, R. D. Farley and G. J. Hutchings, *Phys. Chem. Chem. Phys.*, 2001, **3**, 1073–1080.
44 C. Bolm, M. Martin, G. Gescheidt, C. Palivan, D. Neshchadin, H. Bertagnolli, M. Feth, A. Schweiger, G. Mitrikas and J. Harmer, *J. Am. Chem. Soc.*, 2003, **125**, 6222–6227.
45 C. Bolm, M. Martin, G. Gescheidt, C. Palivan, T. Stanoeva, H. Bertagnolli, M. Feth, A. Schweiger, G. Mitrikas and J. Harmer, *Chem.–Eur. J.*, 2007, **13**, 1842–1850.
46 E. R. Davies, *Phys. Lett. A*, 1974, **A47**, 1–2.
47 P. Hofer, A. Grupp and M. Mehring, *Phys. Rev. A*, 1986, **33**, 3519–3522.
48 C. Remenyi, R. Reviakine, A. V. Arbuznikov, J. Vaara and M. Kaupp, *J. Phys. Chem. A*, 2004, **108**, 5026–5033.
49 S. Kababya, J. Nelson, C. Calle, F. Neese and D. Goldfarb, *J. Am. Chem. Soc.*, 2006, **128**, 2017–2029.
50 C. Remenyi, R. Reviakine and M. Kaupp, *J. Phys. Chem. B*, 2007, **111**, 8290–8304.
51 S. Vancoillie, J. Chalupsky, U. Ryde, E. I. Solomon, K. Pierloot, F. Neese and L. Rulisek, *J. Phys. Chem. B*, 2010, **114**, 7692–7702.
52 J. Gauss, M. Kallay and F. Neese, *J. Phys. Chem. A*, 2009, **113**, 11541–11549.
53 S. Stoll and A. Schweiger, *J. Magn. Reson.*, 2006, **178**, 42–55.
54 P. Hoefer, A. Grupp, H. Nebenfuehr and M. Mehring, *Chem. Phys. Lett.*, 1986, **132**, 279–282.

55 P. Hofer, *J. Magn. Reson., Ser. A*, 1994, **111**, 77–86.
56 C. Gemperle, G. Aebli, A. Schweiger and R. R. Ernst, *J. Magn. Reson.*, 1990, **88**, 241–256.
57 A. Pöppl, M. Hartmann, W. Böhlmann and R. Böttcher, *J. Phys. Chem. A*, 1998, **102**, 3599–3606.
58 A. D. Becke, *Phys. Rev. A*, 1988, **38**, 3098–3100.
59 A. D. Becke, *J. Chem. Phys.*, 1993, **98**, 1372–1377.
60 A. D. Becke, *J. Chem. Phys.*, 1993, **98**, 5648–5652.
61 R. Ahlrichs, M. Bar, M. Haser, H. Horn and C. Kolmel, *Chem. Phys. Lett.*, 1989, **162**, 165–169.
62 A. Schafer, C. Huber and R. Ahlrichs, *J. Chem. Phys.*, 1994, **100**, 5829–5835.
63 ORCA – an *ab initio*, Density Functional and Semiempirical Program Package, 2.5–20.
64 M. Kaupp, R. Reviakine, O. L. Malkina, A. Arbuznikov, B. Schimmelpfennig and V. G. Malkin, *J. Comput. Chem.*, 2002, **23**, 794–803.
65 F. Neese, *J. Phys. Chem. A*, 2001, **105**, 4290–4299.
66 F. Neese, *J. Chem. Phys.*, 2003, **118**, 3939–3948.
67 S. Huzinaga, *Approximate Atomic Functions*, University of Alberta Edmonton, Canada, 1971.
68 W. Kutzelnigg, U. Fleischer, M. Schindler, P. Diehl, E. Fluck, H. Günther, R. Kosfeld and J. Seelig, *NMR Basic Principles and Progress*, Springer-Verlag, Berlin, 1990, vol. 23.
69 F. Neese, *Inorg. Chim. Acta*, 2002, **337**, 181–192.
70 D. A. Evans, E. J. Olhava, J. S. Johnson and J. M. Janey, *Angew. Chem., Int. Ed.*, 1998, **37**, 3372–3375.
71 D. A. Evans, S. J. Miller, T. Lectka and P. von Matt, *J. Am. Chem. Soc.*, 1999, **121**, 7559–7573.
72 M. Orio, O. Jarjayes, H. Kanso, C. Philouze, F. Neese and F. Thomas, *Angew. Chem., Int. Ed.*, 2010, **49**, 4989–4992.
73 J. W. Whittaker, *Chem. Rev.*, 2003, **103**, 2347–2363.
74 A. Livieri, M. Boiocchi, G. Desimoni and G. Faita, *Chem.–Eur. J.*, 2011, **17**, 516–520.
75 C. Foltz, M. Enders, S. Bellemin-Laponnaz, H. Wadepohl and L. H. Gade, *Chem.–Eur. J.*, 2007, **13**, 5994–6008.
76 M. Kruck, D. C. Sauer, M. Enders, H. Wadepohl and L. H. Gade, *Dalton Trans.*, 2011, **40**, 10406–10415.